Aalborg Universitet

AALBORG UNIVERSITY
DENMARK

Shape Modeling of a Concentric-tube Continuum Robot

Bai, Shaoping; Xing, Charles Chuhao

Published in:
Proceedings of the 2012 IEEE International Conference on Robotics and Biomimetics (ROBIO 2012), December 11-14, 2012, Guangzhou, China

DOI (link to publication from Publisher):
10.1109/ROBIO.2012.6490953

Publication date:
2012

Document Version
Early version, also known as pre-print

Link to publication from Aalborg University

Citation for published version (APA):
Bai, S., & Xing, C. C. (2012). Shape Modeling of a Concentric-tube Continuum Robot. In *Proceedings of the 2012 IEEE International Conference on Robotics and Biomimetics (ROBIO 2012), December 11-14, 2012, Guangzhou, China* (pp. 116-121). IEEE. https://doi.org/10.1109/ROBIO.2012.6490953

General rights
Copyright and moral rights for the publications made accessible in the public portal are retained by the authors and/or other copyright owners and it is a condition of accessing publications that users recognise and abide by the legal requirements associated with these rights.

? Users may download and print one copy of any publication from the public portal for the purpose of private study or research.
? You may not further distribute the material or use it for any profit-making activity or commercial gain
? You may freely distribute the URL identifying the publication in the public portal ?

Take down policy
If you believe that this document breaches copyright please contact us at vbn@aub.aau.dk providing details, and we will remove access to the work immediately and investigate your claim.

Downloaded from vbn.aau.dk on: December 25, 2020

Proceedings of the 2012 IEEE
International Conference on Robotics and Biomimetics
December 11-14, 2012, Guangzhou, China

Shape Modeling of a Concentric-tube Continuum Robot

Shaoping Bai[†,‡] and Chuhao Xing[†]
[†]Department of Mechanical and Manufacturing Engineering &
[‡]Centre for Robotics Research
Aalborg University, Aalborg, Denmark
e-mail: shb@m-tech.aau.dk

***Abstract*— Concentric-tube continuum robots feature with simple and compact structures and have a great potential in medical applications. The paper is concerned with the shape modeling of a type of concentric-tube continuum robot built with a collection of super-elastic NiTiNol tubes. The mechanics is modeled on the basis of energy approach for both the in-plane and out-plane cases. The torsional influences on the shape of the concentric-tube robots are considered. An experimental device was build for the model validation. The results of simulation and experiments are included and analyzed.**

Keywords: Flexible manipulators, continuum robots, NiTiNol tubes, mechanics model

I. Introduction

Continuum robots encompass new principles of robot design and construction that are inspired by the nature. The robots are able to move in any direction, both laterally and axially, or even 'turning corner', in a similar manner like elephant trunks or octopus arms. Contrary to traditional robots built with rigid links and joints, a continuum robot is constructed with a collection of flexible structures which allow them deform locally to generate desired motion.

The continuum robots have been attracting more attentions in recent years with a number of prototypes built, including multi-sectional pneumatic actuating robot Air-Octor[1], fluid-driven Octpus Arm[2], tendon-driven robots[3], among others. More efforts were dedicated to robots with concentric tubes of NiTiNol alloy, which are more promising for robotic surgery, due to the relative simple structure, compact size (diameters can be as small as a few millimeters), and bio compatible to human tissues. A number of modeling works on continuum robots can be found in literature [4], [5], [6]. The models were mainly developed on the basis of Cosserat rod with either energy approach or variational methods [7], [8]. In most works, a simplified approach by ignoring the torsional deformation in the robots of concentric tubes were adopted. An approach of including torsion was proposed by Dupont et al. in[9].

In this work, we address the problem of shape modeling for continuum robots built with concentric tubes. The focus is on the torsional deformation of the assembly of tubes. A model of the shape generation is developed. Both simulation and experiment were carried out for model analysis and verification. The experimental results reveal the influence of internal force on the torsional deformation.

The reported work is related to the development of medical robotic systems. While robotic surgical systems, represented by the state-of-the-art da Vinci system from the Intuitive Surgery (http://www.intuitivesurgical.com/), have been successfully and increasingly used in minimal invasive surgeries (MIS), some limitations are experienced by surgeons. One major limitation, taking laparoscopic surgery as example, is the limited mobility within body cavity with the straight-shape instruments, as demonstrated in Fig. 1. The limitation leads to a poor accessibility to deeper body structures thus multiple incisions have to be created, which implies long operation hours in instrument manipulation during operation and slow body recovery thereafter. This limitation becomes more obvious, when robotic surgery is moving to new procedure with single port access (SPA) operations, aiming at decreased recovery time, blood loss, and shortening the length of a patient's hospital staying. A flexible robot like the continuum robot in this study, along with the rigid robot manipulator, is expected to breakthrough the limit on the motion in a confined space, and hence bring a big difference to the medical procedures.

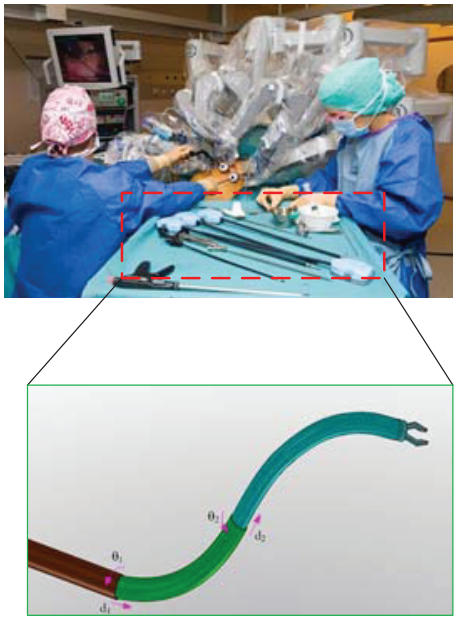

Fig. 1. A da Vinci training robot with straight-shape instruments, comparing with a continuum robot

978-1-4673-2126-6/12/$31.00 © 2012 IEEE

II. Model of a Concentric-Tube Robot

In reality, a concentric robot can be built with multi-sectional tubes, each section being one 'link'. In this work, we confined the modeling work to one-link robot only, which means there are only two tubes that are used.

A. In-Plane Tube Shape Modeling

We start the shape modeling from a simple case, the in-plane case, which means the natural planes of curvature of the tubes are aligned. Another case, the out-plane configuration, is to be described in II-B.

In the in-plane case, the robot is built with tubes of constant pre-curvatures, as demonstrated in Fig.2. After the two tubes are combined together, due to their different curvatures, the two tubes will interfere with one another, causing bending in each other and thus making the shape of combined tubes different from the free shape of the individual tubes. The new shape of the combined tubes can be determined with the energy approach. Assuming two tubes, namely, Tube 1 and Tube 2, have bending stiffness and curvatures E_iI_i and $\kappa_i, i = 1, 2$, respectively, with E_i and I_i denoting the Young's modulus and the area moment of inertia of a cross-section, the total elastic energy for tubes of arc length of $l_i, i = 1, 2$, can be written as

$$U(\kappa) = \frac{1}{2}E_1I_1l_1(\kappa - \kappa_1)^2 + \frac{1}{2}E_2I_2l_2(\kappa - \kappa_2)^2 \quad (1)$$

where κ is the curvature of the tube assembly. Differentiating both sides of equation (1) with respect to κ yields:

$$\frac{dU(\kappa)}{d\kappa} = (E_1I_1l_1 + E_2I_2l_2)\kappa - (E_1I_1l_1\kappa_1 + E_2I_2l_2\kappa_2) \quad (2)$$

The equilibrium condition implies that $dU(\kappa)/d\kappa = 0$, which leads to the solution of κ

$$\kappa = \frac{E_1I_1l_1\kappa_1 + E_2I_2l_2\kappa_2}{E_1I_1l_1 + E_2I_2l_2} \quad (3)$$

In an assembly $l_1 = l_2 = l$, Eq. (3) is simplified as

$$\kappa = \frac{E_1I_1\kappa_1 + E_2I_2\kappa_2}{E_1I_1 + E_2I_2} \quad (4)$$

or

$$\kappa = \frac{1}{E_1I_1 + E_2I_2}(E_1I_1\kappa_1 + E_2I_2\kappa_2) \quad (5)$$

B. Out-Plane Tube Shape Modeling without Torsion

In the out-plane case, as shown in Fig. 3, the two tubes are both rotated with a certain angle from their original position in the x–z plane, before the two tubes are assembled together. The initial angular offsets of Tubes 1 and 2 are θ_1 and θ_2, respectively. After the two tubes are combined together, the equilibrium position is reached in the plane of angular offset ϕ from the x–z plane.

In order to describe the out-plane shape of the pre-curved tubes, we decompose the curvature of each tube in

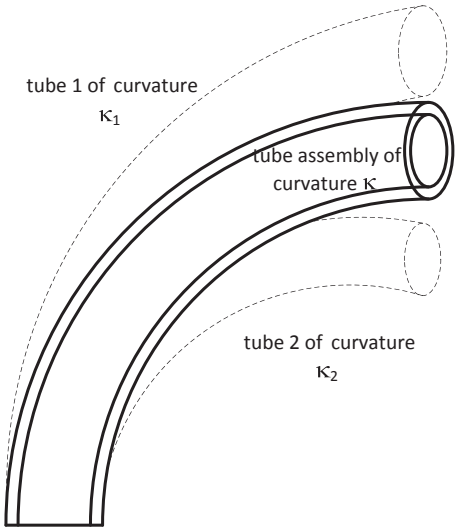

Fig. 2. Two tubes being combined together to a concentric tube

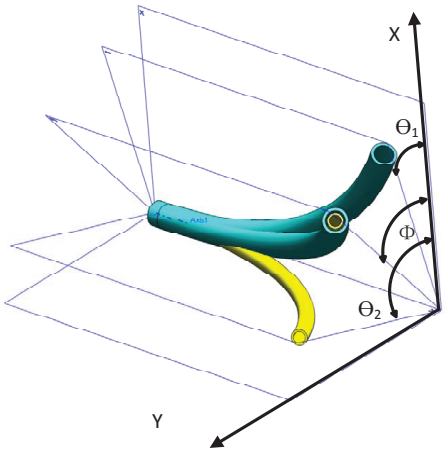

Fig. 3. Two tubes in different planes combined to build a concentric tube

3D space into two components so that they comply with the constitutive law in 3D curved beam. The two components decomposed are

$$\kappa_{ix} = \kappa_i \cos\theta_i; \quad \kappa_{iy} = \kappa_i \sin\theta_i \quad (6)$$

Such decomposition does not have any geometric implication, i.e., the components does not correspond to the curvatures of tubes projection in two plane, namely, x–z and y–z planes.

Neglecting the elastic energy caused by torsion, the total elastic energy of the over-lapping tubes shown in Fig. 3 can be written as:

$$\begin{aligned} U =& \frac{1}{2}E_1I_1l_1(\kappa_x - \kappa_{1x})^2 + \frac{1}{2}E_2I_2l_2(\kappa_x - \kappa_{2x})^2 \\ &+ \frac{1}{2}E_1I_1l_1(\kappa_y - \kappa_{1y})^2 + \frac{1}{2}E_2I_2l_2(\kappa_y - \kappa_{2y})^2 \end{aligned} \quad (7)$$

where κ_x, κ_y are the two components of the curvature of the assembly decomposed follow the same way as equation (6). To find out the minimum of the total elastic energy, differentiating Eq. (7), and set the partial derivatives to zero,

which gives:

$$\frac{\partial U(\kappa_x,\kappa_y)}{\partial \kappa_x}=0, \quad \frac{\partial U(\kappa_x,\kappa_y)}{\partial \kappa_y}=0 \tag{8}$$

Equation (8) yields:

$$\kappa_x=\frac{E_1I_1l_1\kappa_{1x}+E_2I_2l_2\kappa_{2_x}}{E_1I_1l_1+E_2I_2l_2} \tag{9}$$

$$\kappa_y=\frac{E_1I_1l_1\kappa_{1y}+E_2I_2l_2\kappa_{2_y}}{E_1I_1l_1+E_2I_2l_2} \tag{10}$$

The curvature of the assembly is

$$\kappa=\sqrt{\kappa_x^2+\kappa_y^2} \tag{11}$$

For an assembly $l_1=l_2=l$, substituting eq. (6) into eqs.(9) and (10) leads to

$$\kappa_x=\frac{E_1I_1\kappa_1\cos\theta_1+E_2I_2\kappa_2\cos\theta_2}{E_1I_1+E_2I_2} \tag{12}$$

$$\kappa_y=\frac{E_1I_1\kappa_1\sin\theta_1+E_2I_2\kappa_2\sin\theta_2}{E_1I_1+E_2I_2} \tag{13}$$

The offset angle of the equilibrium plane ϕ can be obtained with:

$$\phi=\tan^{-1}(\frac{\kappa_y}{\kappa_x}) \tag{14}$$

Equations (12) and (13) can be written in a compact form

$$\boldsymbol{\kappa}=(\mathbf{K}_1+\mathbf{K}_2)^{-1}(\mathbf{R}_z(\theta_1)\mathbf{K}_1\bar{\boldsymbol{\kappa}}_1+\mathbf{R}_z(\theta_2)\mathbf{K}_2\bar{\boldsymbol{\kappa}}_2) \tag{15}$$

where $\mathbf{R}_z$ is the 2D rotation matrix about z axis, and

$$\bar{\boldsymbol{\kappa}}_i=\begin{bmatrix}\kappa_i\\0\end{bmatrix}, \quad \mathbf{K}_i=\begin{bmatrix}E_iI_i & 0\\0 & E_iI_i\end{bmatrix}, i=1,2 \tag{16}$$

III. Out-Plane Tube Shape Modeling with Torsion

A major limitation with eqs.(12) and (13) is that the model doesn't account for the torsion in the tubes, in another word, it is a torsionally rigid model. The model to some extents leads to inaccurate results in pose calculation. Moreover, the decomposition in the way of eq. (6) is not geometrically meaningful. In light of this, the model is further developed to incorporate with the torsional deformation by resorting the approach proposed by Dupont [9].

We first introduce arc length s as parameter to describe the tube position, such that any point can be expressed as $\mathbf{r}=\mathbf{r}(s)$. Further more, we define $\theta_i(s)$ as the twist angle of tube i at section s.

For out-plane tubes, the curvature is not constant as the in-plane case. Instead, the curvature varies with the arc length. Accordingly, the curve's shape can be determined by a vector of curvature at a point $\mathbf{r}(s)$ along the tubes centerline. Let

$$\boldsymbol{\kappa}_i(s)=\begin{bmatrix}\kappa_{ix}\\\kappa_{iy}\\\tau_i\end{bmatrix} \tag{17}$$

be the curvature-torsion vector, where $(\kappa_{ix},\kappa_{iy})$ are the components of curvature due to bending, and τ_i is the changing rate of torsion angle, i.e., $\tau_i=d\theta_i/ds$. Note that a curve with $\tau=0$ anywhere is a plane curve, which is the case of in-plane tubes.

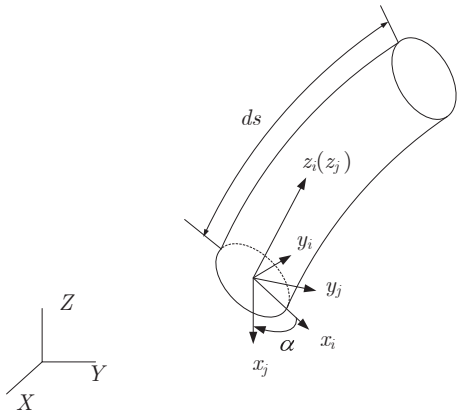

Fig. 4. Local frames at a cross-section of the tube assembly

When two tubes are assembled, they build a constrained mechanical system, in which the internal moments are balanced and, geometrically, two tubes' center lines superposition each other with only difference in torsional twist. The two constrains can be described by

$$\mathbf{m}_1(s)-\mathbf{R}_z(\alpha)\mathbf{m}_2(s)=0 \tag{18}$$

$$\boldsymbol{\kappa}_1(s)-\mathbf{R}_z(\alpha)\boldsymbol{\kappa}_2(s)+\dot{\alpha}(s)\mathbf{e}_z=0 \tag{19}$$

where $\mathbf{e}_z=[0,0,1]^T$, $\mathbf{m}_i(s)$ is the three-component bending moment vector of the ith tube, and α is the relative twist angle demonstrated in Fig.4, which is defined as the difference between the twist angles of two tubes as

$$\alpha(s)=\theta_2(s)-\theta_1(s) \tag{20}$$

It is noted that all moments in eq.(18) are expressed in local components.

The moments, either internal or external ones, will cause curvature changes with the tube. Assuming the tube deformation is linear, the bending moment vector $\mathbf{m}_i(s)$ at any section s along the ith tube can be written as

$$\mathbf{m}_i(s)=\mathbf{K}_i\delta\boldsymbol{\kappa}_i \tag{21}$$

where stiffness matrix $\mathbf{K}_i$, $i=1,2$, are expanded to three dimensions, i.e.,

$$\mathbf{K}_i=\begin{bmatrix}k_{ix}&0&0\\0&k_{iy}&0\\0&0&k_{iz}\end{bmatrix}=\begin{bmatrix}E_iI_i&0&0\\0&E_iI_i&0\\0&0&J_iG_i\end{bmatrix} \tag{22}$$

The change in the curvature-torsion vector can be found from the differential geometry. A simplified expression of $\delta\boldsymbol{\kappa}_i$ is given by

$$\delta\boldsymbol{\kappa}_i=\boldsymbol{\kappa}_i(s)-\bar{\boldsymbol{\kappa}}_i(s) \tag{23}$$

where $\bar{\boldsymbol{\kappa}}_i(s)$ be the initial or pre-curvature vector of ith tube. If we assume the pre-curvatures of the tubes are constant through out the arc, the pre-curvature vector of ith tube $\bar{\kappa}_i(s)$

can now be simplified to $\bar{\kappa}_i$, that is

$$\bar{\kappa}_i = \begin{bmatrix} \bar{\kappa}_{ix} \\ \bar{\kappa}_{iy} \\ \bar{\kappa}_{iz} \end{bmatrix} \tag{24}$$

The bending moment vector $\mathbf{m}_i(s)$ varies as a function of s, which variation, according to the theory of linear elasticity, can be described by

$$\mathbf{m}_i'(s) + \boldsymbol{\kappa}_i(s) \times \mathbf{m}_i(s) + \mathbf{e}_z \times \mathbf{f}_i(s) = \mathbf{0} \tag{25}$$

where $\mathbf{f}_i(s)$ is the shear force at the cross-section.

Now we have a system of differential-algebraic equations (DAE). To solve the equations, we first make use of the constitutive law of eq. (21). Differentiating both sides of eq. (21) with respect to s yields

$$\mathbf{m}_i'(s) = \mathbf{K}_i \boldsymbol{\kappa}_i'(s) \tag{26}$$

After substituting eqs (21) and (26) into eq. (25), the third equation of eq. (25) becomes

$$G_i J_i \tau_i' = E_i I_i [\kappa_{iy}(\kappa_{ix} - \bar{\kappa}_{ix}) - \kappa_{ix}(\kappa_{iy} - \bar{\kappa}_{iy})] \tag{27}$$

Noting $\tau_i = \theta_i'(s)$, Eqs. (20) and (27) lead to

$$\begin{aligned} \alpha''(s) =& \frac{E_2 I_2}{G_2 J_2}[\kappa_{2y}(\kappa_{2x} - \bar{\kappa}_{2x}) - \kappa_{2x}(\kappa_{2y} - \bar{\kappa}_{2y})] \\ & - \frac{E_1 I_1}{G_1 J_1}[\kappa_{1y}(\kappa_{1x} - \bar{\kappa}_{1x}) - \kappa_{1x}(\kappa_{1y} - \bar{\kappa}_{1y})] \end{aligned} \tag{28}$$

The solutions of κ_{ix} and κ_{iy} can be found from the system of algebraic equations, namely, the moment equilibrium equation (18), the constitutive model (21) and the compatibility equation (19). Substituting the expressions of κ_{ix} and κ_{iy} into eq. (28) and simplifying the obtained equation yields

$$\alpha''(s) = A \sin \alpha(s) + B \cos \alpha(s) \tag{29}$$

with

$$\begin{aligned} A =& \frac{E_2 I_2 E_1 I_1}{G_1 J_1 G_2 J_2 (E_1 I_1 + E_2 I_2)}(-J_1 G_1 \bar{\kappa}_{1y} \bar{\kappa}_{2x} \\ & + J_1 G_1 \bar{\kappa}_{1x} \bar{\kappa}_{2y} + J_2 G_2 \bar{\kappa}_{2y} \bar{\kappa}_{1x} - J_2 G_2 \bar{\kappa}_{2x} \bar{\kappa}_{1y}) \end{aligned} \tag{30}$$

$$\begin{aligned} B =& \frac{E_2 I_2 E_1 I_1}{G_1 J_1 G_2 J_2 (E_1 I_1 + E_2 I_2)}(J_1 G_1 \bar{\kappa}_{1x} \bar{\kappa}_{2x} \\ & + J_1 G_1 \bar{\kappa}_{1y} \bar{\kappa}_{2y} + J_2 G_2 \bar{\kappa}_{2x} \bar{\kappa}_{1x} + J_2 G_2 \bar{\kappa}_{2y} \bar{\kappa}_{1y}) \end{aligned} \tag{31}$$

Differential equation (29) can be solved with boundary conditions. At the input side ($s = 0$),

$$\alpha(0) = \theta_2(0) - \theta_1(0) \tag{32}$$

while at the output side ($s = l$),

$$\dot{\alpha}(l) = 0 \tag{33}$$

.

Upon the solution of $\alpha(s)$, the curvature of Tube 2 can be obtained

$$\kappa_2 = (\mathbf{K}_1 + \mathbf{K}_2)^{-1} {\mathbf{R}_z}^T(\alpha) \mathbf{K}_1 \bar{\boldsymbol{\kappa}}_1 + \mathbf{K}_2 \bar{\boldsymbol{\kappa}}_2 + \dot{\alpha} \mathbf{K}_1 \mathbf{e}_z \tag{34}$$

The curvature-torsion vector of Tube 1, on the other hand, is different from Tube 2 in the rate of torsion only.

With the curvature and the changing rate of torsion angle, the tubes's shape can be determined by

$$\mathcal{C}(s) = \mathbf{x}_0 + \int_0^s \mathbf{v}_1(v) dv \tag{35}$$

$$= \mathbf{x}_0 + \int_0^s (\mathbf{v}_{10} + \int_0^u \frac{d\mathbf{v}_1}{du} du) dv \tag{36}$$

where $\mathbf{v}_1$ is the tangential vector of the centerline curve, with $\mathbf{v}_{10}$ being the tangential vector at the base point, i.e., at point $s = 0$. The Frenet-Serret equations are used to find the tangential vector

$$\frac{d\mathbf{v}_1}{ds} = \kappa(s) \mathbf{v}_2(s) \tag{37}$$

$$\frac{d\mathbf{v}_2}{ds} = -\kappa(s) \mathbf{v}_1(s) + \tau(s) \mathbf{v}_3(s) \tag{38}$$

$$\frac{d\mathbf{v}_3}{ds} = -\tau(s) \mathbf{v}_2 \tag{39}$$

where $\mathbf{v}_2$ is the unit normal vector and $\mathbf{v}_3 = \mathbf{v}_1 \times \mathbf{v}_2$. Note that the subscripts of tubes are omitted for clarity.

So far, we have the shape model of concentric tubes.

IV. Simulation

The material of the concentric tubes is NiTiNol (Nickel-Titanium) alloy, a kind of NiTi-based materials with the composition of almost equal amount of Nickel and Titanium. Due to the properties of super-elasticity and shape-memory effect, together with high fatigue resistance and bio-compatibility, the NiTiNol is an ideal material in the medical industries.

A. Material properties

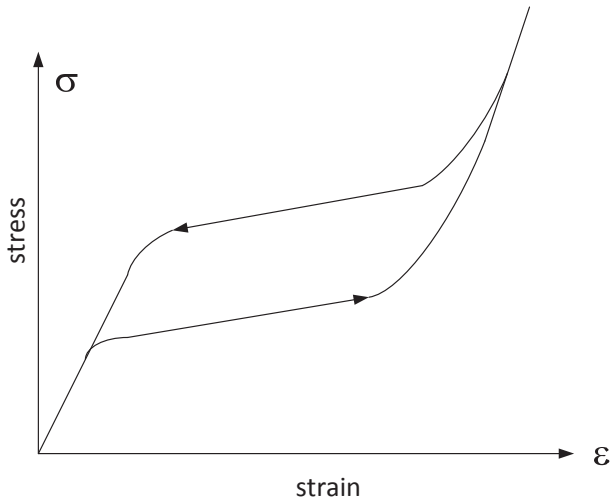

Fig. 5. Stress-strain relationship of NiTiNol tubes

The NiTiNol is a super-elasticity material, which means it is able to undergo large elastic deformation. The stress-strain behavior of NiTiNol is shown in Fig.9, noting that the stress-strain curve is recorded when the NiTiNol is under both loading and unloading. Hysteresis property can be observed. In terms of elasticity, the NiTiNol remains elastic even up to 8% of strain. However, super-elasticity only exist over a relatively narrow temperature range above

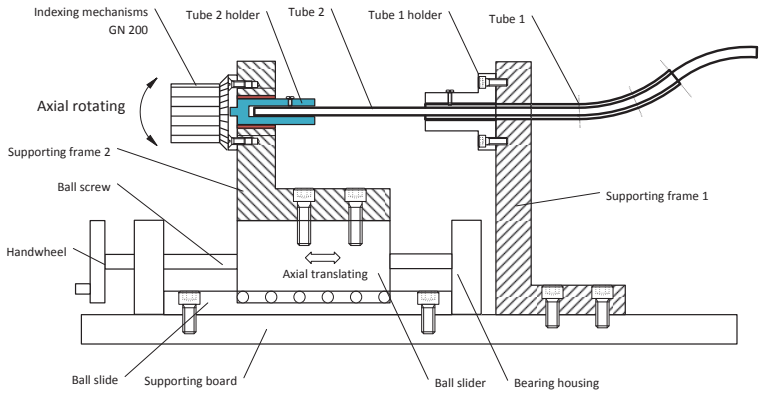

Fig. 6. Assembly drawing of the manual-actuated testing device

the A_f temperature(optimum performance at A_f temperature). Moreover, the stiffness of the NiTiNol changes with temperature at a rate of about $4-8MPa/^oC$. The variability of elasticity with temperature is a main bottleneck to the application of NiTiNol. Despite of the temperature limits of elasticity, when applied in medical situation, where the human body temperature is around 37^oC, the NiTiNol can maintain superelastic as well as maintain a relatively stable stiffness.

B. Tube Selection

As revealed by equations (18) and (19), the kinematics of the concentric-tube robot is subject to the stiffness and curvatures. To enable the robot have desired compliance, the tube dimensions, including tube diameter, wall thickness, and materials have to be selected carefully. The feasible NiTiNol tubes from EUROFLEX GmbH range from $0.4mm$ to $10mm$. To avoid local buckling in making the pre-curvature at room temperature, as well as to save cost, we consider the following criteria in selecting tubes:

- The diameter/thickness ratio is smaller than 15.
- The diameter of the tube is smaller than $5mm$ and larger than $1.3mm$.

Table I lists some available tubes from the supplier EUROFLEX GmbH. Taking into considerations of clearance, Tubes #2 and #3 were selected for testing. The selected tubes

TABLE I
FEASIBLE TUBES PARAMETERS

Tube	d(outer dia.)	t(thickness)	Model	$r = d/t$
#1	3.084	0.279 mm	NiTi SE 508	11.1
#2	2.591	0.292 mm	NiTi SE 508	8.9
#3	1.600	0.200 mm	NiTi SE 508	8.0
#4	1.320	0.225 mm	NiTi SE 508	5.9

were bent plastically using a tube bender to give the tubes the pre-curvatures. Care is given to the bending process to avoid rotating the tube, so that the tube will remain in one plane.

C. Simulations

With the selected tubes, simulations were conducted for the inputs in the range of [0, 360] degree. The parameters of simulation are listed in Table II. The vector of initial curvature is $\bar{\boldsymbol{\kappa}}_i = [\kappa_i, 0, 0]^T$.

TABLE II
SIMULATION PARAMETERS

Parameter	Value	Description
E	$7 \times 10^{10} Pa$	Young's Modulus
G	$2.3 \times 10^{10} Pa$	Shear Modulus
κ_1, κ_2[1/mm]	$1/236, 1/294$	pre-curvature
l_1, l_2	$200, 200$ [mm]	tube length

The torsional twists at the distal end were found numerically from the analytical equation (29). The results are displayed in Fig. 8. It can be seen from the simulation that the twist varies periodically with a period of 360 degrees. At points of input twists being equal to multiples of 180 degrees, the two tubes become co-planar, which agrees with phenomenon that can be observed.

V. EXPERIMENTAL VERIFICATION

A concept of 2-DOF continuum robot was proposed. As demonstrated in Fig.6, two tubes are mounted in a platform, one fixed and another is able to translate and rotate with respect to the grounded frame, in order to control the the rotation at the distal end. The position of the ball slider is controlled by the hand wheel. By turning the hand wheel the ball screw mechanism translates the rotation of the hand wheel into the translation of the ball slider.

A. Mechanical design

In this work, the robot was used for testing the torsional deformation. To this end, an indexing mechanism GN200 with a shaft key replaced the motor to rotate the tube 2.

The testing device built, shown in Fig. 7, is constructed with standard parts including the indexing mechanism GN200 and bearing housings (pillow block). The rest parts were all made in the workshop at university. The structural frames of the device are made of aluminum, except for the tube holders, which are made of steel to have sufficient hardness to hold the NiTiNol tubes.

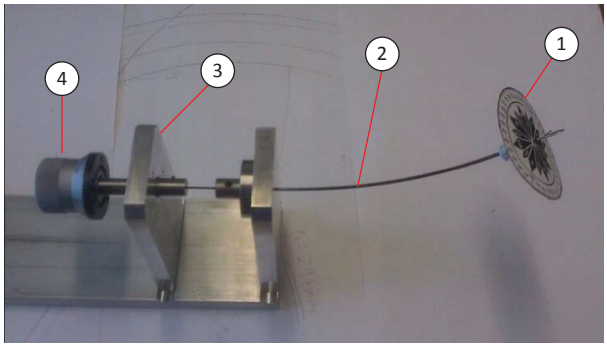

Fig. 7. Test setup for torsional twist, (1) circular graduated disk, (2) assembly of tubes, (3) mounting frame, (4) indexing mechanism.

B. Measurements

In the torsional measurement, two parameters are concerned, one is the rotational input, another one is the twist at the distal end. The input can be measured from the reading of the indexing mechanism. For the twist output, a circular graduated disk was mount to the outer tube, while a pointer is firmly inserted into the inner tube. The resolutions of both indexing mechanism and the graduated disk are 1 degree.

The torsional tests were conducted for the input range of [0, 360]degree. The inner tube was rotated first counter clockwisely and then clockwisely. The measurement was repeated for three times.

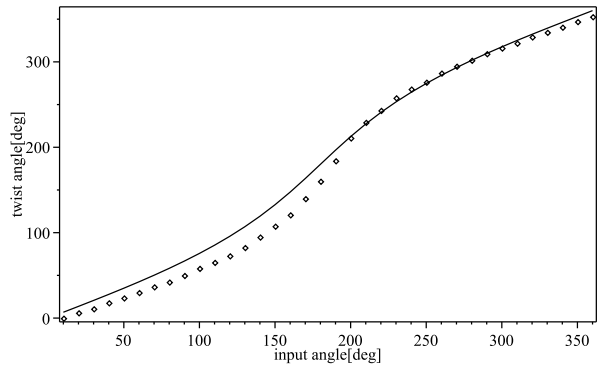

Fig. 8. Simulation (solid lines) and measurement (dots) results of twist angles

The twist angles at the distal end, which varies as a function of input angles, are plotted in Fig. 8. The angles are averaged with the three measurements of forward rotations. The results show good agreements with the simulations.

Figure 9 shows the measured twist angles for both forward and reverse rotations. The difference in the twist angles for the same inputs but different in rotation directions is noticeable. The maximum difference for the same input angle is found as 14 degrees, or 3.9% of the full scale. The difference is the results of hysteresis characteristics of the NiTiNol materials. As shown in Fig.5, the stress is not linear to the stress for a certain range of strains. Moreover, the frictional force between two tubes also contributes to the difference. The inclusion of frictional influence in the shaping modeling remains an open problem.

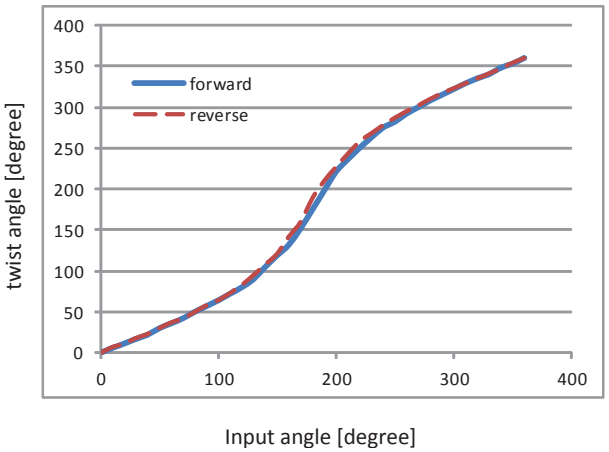

Fig. 9. Measurement of twist angles with forward and reverse rotations at input

VI. Conclusions

In this work, the shape modeling of a type of concentric-tube continuum robot was developed for a collection of super-elastic NiTiNol tubes. The mechanics was modeled on the basis of energy approach for both the in-plane and out-plane cases. Special attention was given to the torsional influences on the shape of the concentric-tube robots. An experimental device was built for the model validation. The results reveal the good agreement between the model simulation and measurements.

The future work includes the further development of the shape model of the continuum robot with a simplified approach for the motion control purpose. The measurement of 3D motion will also be considered.

References

[1] M. Blessing and I.D. Walker. Novel continuum robots with variable-length sections. In *Proc. 3rd IFAC Symposium on Mechatronic Systems, Sydney, Australia*, 2004.

[2] B. Mazzolai, L. Margheri, M. Cianchetti, P. Dario, and C. Laschi. Soft-robotic arm inspired by the octopus: II. from artificial requirements to innovative technological solutions. *Bioinspiration & Biomimetics*, 7(2):025005, 2012.

[3] C. Li. *Design of Continuous Backbone, Cable-driven Robots*. Clemson University, 2000.

[4] P. E. Dupont, J. Lock, and E. Butler. Torsional kinematic model for concentric tube robots. In *Proc. 2009 IEEE Inter. Conf. on Robotics and Automation*, pages 2964–2971, 2009.

[5] Robert J. Webster, III and Bryan A. Jones. Design and kinematic modeling of constant curvature continuum robots: A review. *Int. J. Robotics Research*, 29(13):1661–1683, 2010.

[6] B. A. Jones, R. L. Gray, and K. Turlapati. Three dimensional statics for continuum robotics. In *Proc. 2009 IEEE/RSJ Int. Conf. on Intelligent robots and systems*, pages 2659–2664, 2009.

[7] D. B. Camarillo, C. F. Milne, C. R. Carlson, M. R. Zinn, and J. K. Salisbury. Mechanics modeling of tendon-driven continuum manipulators. *IEEE Trans. Robotics*, 24(6):1262–1273, 2008.

[8] H. Lang, J. Linn, and M. Arnold. Multibody dynamics simulation of geometrically exact Cosserat rods. *Multibody Dynamics*, 25:285–312, 2011.

[9] P. E. Dupont, J. Lock, B. Itkowitz, and E. Butler. Design and control of concentric-tube robots. *IEEE Trans. Robotics*, 26(2):209–225, 2010.